Mechanisms of Asian Summer Monsoon Changes in Response to Anthropogenic Forcing in CMIP5 Models*

XIAOQIONG LI

Department of Earth and Environmental Sciences, and Lamont-Doherty Earth Observatory, Columbia University, Palisades, New York

MINGFANG TING, CUIHUA LI, AND NAOMI HENDERSON

Lamont-Doherty Earth Observatory, Columbia University, Palisades, New York

(Manuscript received 8 August 2014, in final form 1 March 2015)

ABSTRACT

Changes of the Asian summer monsoon in response to anthropogenic forcing are examined using observations and phase 5 of the Coupled Model Intercomparison Project (CMIP5) multimodel, multirealization ensemble. In the twentieth century, CMIP5 models indicate a predominantly drying Asian monsoon, while in the twenty-first century under the representative concentration pathway 8.5 (RCP8.5) scenario, monsoon rainfall enhances across the entire Asian domain. The thermodynamic and dynamic mechanisms causing the changes are evaluated using specific humidity and winds, as well as the moisture budget. The drying trend in the CMIP5 historical simulations and the wetting trend in the RCP8.5 projections can be explained by the relative importance of dynamic and thermodynamic contributions to the total mean moisture convergence. While the thermodynamic mechanism dominates in the future, the historical rainfall changes are dominated by the changes in circulation. The relative contributions of aerosols and greenhouse gases (GHGs) on the historical monsoon change are further examined using CMIP5 single-forcing simulations. Rainfall reduces under aerosol forcing and increases under GHG forcing. Aerosol forcing dominates over the greenhouse effect during the historical period, leading to the general drying trend in the all-forcing simulations. While the thermodynamic change of mean moisture convergence in the all-forcing case is dominated by the GHG forcing, the dynamic change of mean moisture convergence in the all-forcing case is dominated by the aerosol forcing.

1. Introduction

With its large population, increasing industrial development, and severe water stresses, Asia is one of the most vulnerable regions in the world facing hydroclimate changes. Piao et al. (2010) assessed the impacts of climate change on water resources and agriculture in China, suggesting a 20% crop production decrease by 2050 under the worst case scenario. However, the overall impact is far from certain because of the high variability and uncertainty in projected climate, particularly precipitation, and the corresponding crop responses. The Asian monsoon is one of the major monsoon systems in the world, with critical importance in terms of climate impacts in Asia and globally (e.g., Rodwell and Hoskins 1996; Liu and Yanai 2001; Lin and Wu 2012). Analyzing and understanding the characteristics of monsoon change has important implications for various socioeconomic sectors and human well-being, including water resource management, agriculture, ecosystem service, food security, and public health (e.g., Krishna Kumar et al. 2004; Hong and Kim 2011; Mirza 2011).

The Asian monsoon is an interactive system influenced by both internal variability and external forcing (e.g., Lei et al. 2011; Turner and Annamalai 2012; Song et al. 2014). There have been extensive observational, modeling, as well as paleoclimate studies on Asian

monsoon variability, particularly on interannual time scales, revealing strong associations with El Niño–Southern Oscillation (e.g., Wang et al. 2000; Krishna Kumar et al. 2006; Lau and Nath 2006; Cook et al. 2010; Mishra et al. 2012). However, anthropogenic factors, particularly the increasing concentration of greenhouse gases (GHGs) and changing aerosol emissions in recent decades and the future, could have profound consequences on monsoon behavior. For the forced change of Asian monsoon during the past century, several studies have addressed the weakening monsoon circulation during the second half of the twentieth century, for both Indian monsoon (Annamalai et al. 2013) and East Asian monsoon (Song et al. 2014). As for future projections, modeling studies suggest intensification of future monsoon under global warming, in both mean precipitation and extreme events (Ueda et al. 2006; Seo et al. 2013; Wang et al. 2014). Understanding how the monsoon may change in the future and why the changes occur is a challenging task for hydroclimate research.

Previous studies have advanced our understanding of the physical mechanisms causing the changes of the hydrological cycle in response to global warming on a global scale. For large-scale changes, the ''wet get wetter'' or ''rich get richer'' mechanism (Held and Soden 2006) emphasizes the thermodynamic effect resulting from the increase in lower-tropospheric water vapor in a warming atmosphere. Based on the Clausius–Clapeyron equation, the amount of saturation vapor pressure increases at a rate of about $7\% \, \mathrm{K}^{-1}$. Consequently, horizontal moisture transport increases within the atmosphere, leading to enhanced precipitation minus evaporation ($P - E$) where mean moisture converges and reduced $P - E$ where moisture diverges. However, precipitation increases are also controlled by the radiative (energy) constraints (e.g., Takahashi 2009; O'Gorman et al. 2012), making the rate of precipitation increase less than the $7\% \, \mathrm{K}^{-1}$. As a consequence, the atmospheric overturning circulation slows down as climate warms, especially for the Walker circulation in the tropics (Vecchi and Soden 2007). Using moisture budget analysis, Seager et al. (2010) show that the global $P - E$ change follows the wet-get-wetter pattern with a large part of this change coming from the thermodynamic component because of the rise in specific humidity. Seager et al. (2010) further show that, in the tropics, circulation changes (dynamic contribution) offset some of the thermodynamic change because of the slowdown of the tropical divergent circulation. Based on an evaluation on tropical regional precipitation change, Chou et al. (2009) find that the thermodynamic component is a good approximation for large-scale averages, but dynamic feedback can substantially increase or decrease

precipitation anomalies within the convergence zones. For spatial distribution of the tropical rainfall response, another fundamental view is the ''warmer get wetter'' mechanism (Xie et al. 2010) over the tropical ocean, suggesting that precipitation increases where the sea surface temperature (SST) warming exceeds the tropical mean and vice versa.

For the mechanisms of Asian monsoon change, rainfall is expected to increase under GHG-induced warming mainly because of more abundant tropospheric water vapor, following the wet-get-wetter mechanism, accompanied by the weakening monsoon circulation (Ueda et al. 2006). Studies using model projections from phases 3 and 5 of the Coupled Model Intercomparison Project (CMIP3 and CMIP5) suggest that the monsoon rainfall is likely to strengthen globally in the future because of enhanced atmospheric moisture and surface evaporation, leading to an increase in moisture convergence (Kitoh et al. 2013; Lee and Wang 2014). In the Asian monsoon region, the dynamical weakening of monsoon circulation is shown to be much lower than that of other monsoons, resulting in a larger rainfall increase (Endo and Kitoh 2014). Greenhouse warming could also induce horizontal thermal contrasts, favoring the Asian monsoon precipitation to increase: the east–west asymmetry in the sea level pressure (SLP) field generated by the ''warmer land–cool ocean'' and the hemispheric SLP difference generated by the ''warm Northern Hemisphere–cool Southern Hemisphere'' (Wang et al. 2014). However, SST warming associated with increasing GHGs over the tropical western Pacific could affect atmospheric circulation and cause a drying trend over South Asia (Annamalai et al. 2013).

Aerosol effect is another major driver of anthropogenic climate change, particularly over Asia, considering its severe air pollution problem in recent years. The possible impacts of aerosols on rainfall have drawn much attention in recent Asian monsoon research (e.g., Bollasina et al. 2011; Ganguly et al. 2012a,b; Wu et al. 2013). Increased aerosol concentration in the atmosphere could reduce the surface solar radiation (''dimming'' effect), which weakens the SST gradient in the Indian Ocean and reduces local Hadley cell circulation, thereby weakening the Indian monsoon (Ramanathan et al. 2005). On the other hand, the ''elevated heat pump'' hypothesis (Lau et al. 2006) suggests that aerosols could enhance the meridional temperature gradient in the middle-to-upper troposphere, causing an advancement and intensification of the Indian summer monsoon rainfall.

Although there is a general consensus on the large-scale thermodynamic mechanism of hydroclimate change, the dynamic response is not well understood.
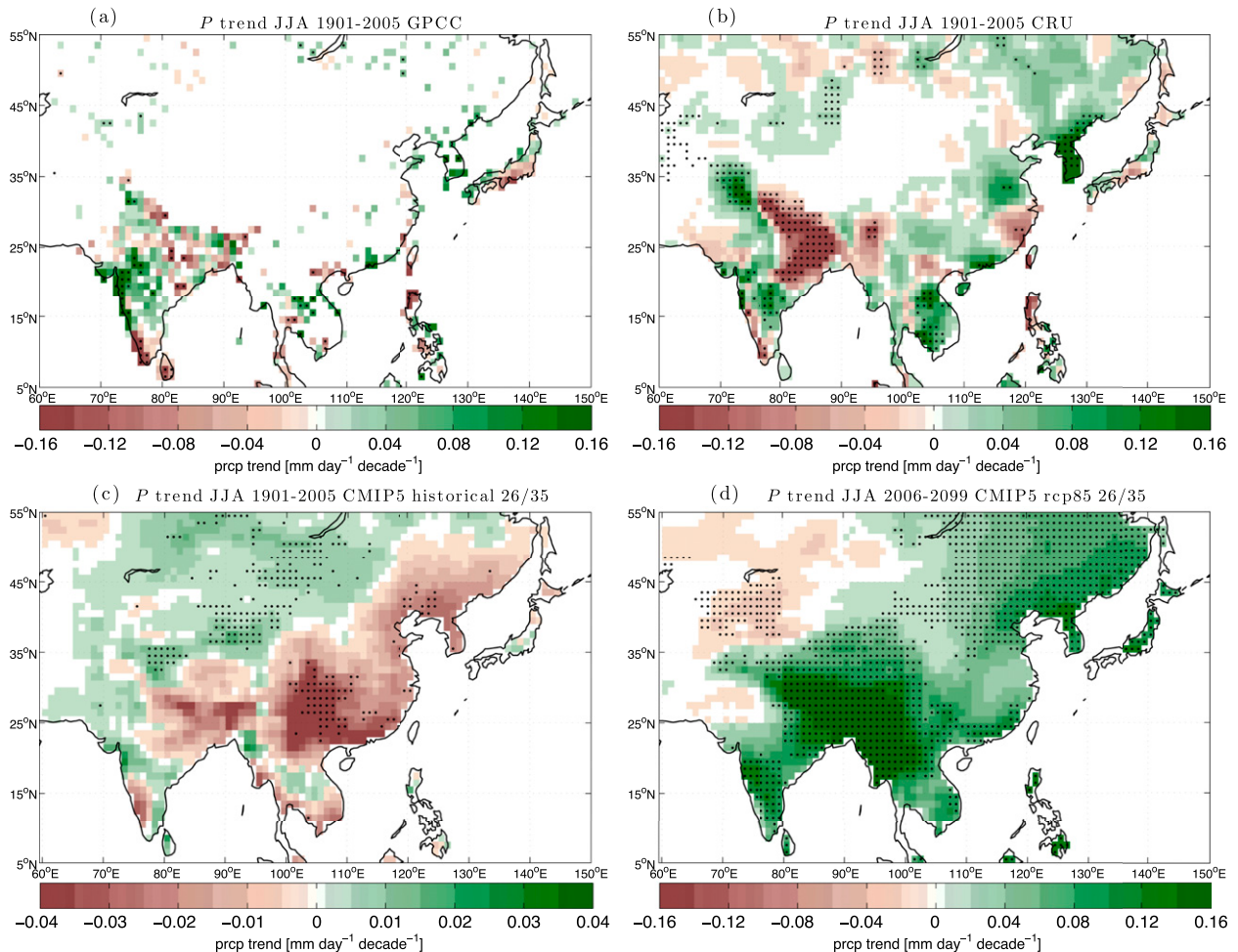
FIG. 1. Linear trend of JJA precipitation (mm day^{-1} decade^{-1}) for (a) GPCC 1901–2005 data, (b) CRU 1901–2005 data, (c) CMIP5 35-model MMM historical 1901–2005 simulations, and (d) CMIP5 RCP8.5 2006–99 simulations. For observations in (a),(b), only the grid boxes where at least one rain gauge existed in any month of the JJA season for at least 80 yr are plotted. Stippling denotes 5% significance based on two-sided Student's t test in (a),(b) and 26 of 35 model agreement in (c),(d).

Furthermore, the effects of climate change on the regional scale, especially monsoon strength and variability, are complex and uncertain (Christensen et al. 2014). The question of how Asian monsoon rainfall and circulation may respond to future anthropogenic forcing, including both aerosols and GHGs, is far from conclusive.

Observed linear trend of Asian summer monsoon rainfall (June–August mean from 1901 to 2005) shows large uncertainty but with a slight wetting trend for the area average (Figs. 1a,b). We used two available rainfall datasets for the estimate of linear trend in Fig. 1, the Global Precipitation Climatology Centre (GPCC; Fig. 1a) and the Climate Research Unit (CRU) at the University of East Anglia (Fig. 1b) (see section 2 for detailed information on these datasets), and the trends are shown only for those grid boxes where at least one

rain gauge existed in any month of the June–August (JJA) season for at least 80 yr. The CMIP5 multimodel simulated linear trend over the same time period presents a dominant drying signal over most of the Asian monsoon region, particularly over China and northeastern India (Fig. 1c). The modeled historical trend (Fig. 1c) shows some similarity with the observations (Figs. 1a,b) over India, while the discrepancy is large over eastern China, where the data coverage is relatively poor. On the other hand, future projection under the representative concentration pathway 8.5 (RCP8.5) emission scenario presents a predominantly wetting trend across the entire monsoon region (Fig. 1d). The discrepancies between observations and model simulations as well as the contrast between past and future changes motivate us to examine further the causal mechanisms and to explore the relative effects of

aerosols and GHGs for the historical period. Given the complex nature of the radiative forcing for the twentieth century with both anthropogenic aerosols and GHGs as well as other natural radiative forcing and the large monsoon variability on interannual and decadal time scales, the linear trend may not be able to accurately represent anthropogenic changes. Thus, it is essential to obtain a better estimate of the forced signal and separate the radiatively forced component for Asian monsoon rainfall from the natural varying component. We used the signal-to-noise (S/N) maximizing empirical orthogonal function (EOF) (Ting et al. 2009) technique in this study to obtain a model-based best estimate of the radiatively forced signal in monsoon rainfall.

We examined Asian summer monsoon patterns in response to anthropogenic forcing for JJA seasonal mean using observations and the CMIP5 multimodel ensemble historical simulations under the all-forcing, aerosol-forcing, and GHG-forcing scenarios and future projections under the RCP8.5 emission scenario. The main focus of this study is to investigate the possible causes of these changes for both the twentieth and twenty-first centuries, including 1) the thermodynamic and dynamic mechanisms and 2) the relative impacts of aerosols and GHGs. The paper is organized as follows: Section 2 describes observed datasets and model simulations used in the study. Section 3 presents methodology of the analysis. Results regarding forced changes of Asian summer monsoon rainfall in the twentieth and twenty-first centuries are shown in section 4, followed by a detailed analysis of the dynamic and thermodynamic mechanisms governing these changes in section 5. The relative roles of aerosols and GHGs in contributing to monsoon rainfall changes during the historical period are discussed in section 6. The main conclusions are summarized in section 7.

2. Data

a. Observational and reanalysis data

We used monthly data from two gridded observational datasets for precipitation: the GPCC full data product, version 6, from the World Climate Research Programme (WCRP) Global Climate Observing System (GCOS) (Schneider et al. 2011) and data from CRU at the University of East Anglia, version 3.2 (Harris et al. 2014). The spatial resolution is $0.5° \times 0.5°$ for both datasets, interpolated to $1° \times 1°$ to allow for a higher rain gauge count within each grid box. Only the grid boxes where at least one rain gauge existed in any month of the JJA season for at least 80 yr during the 1901–2005 period were used in the analysis in order to improve the data

reliability. We used monthly data from the National Oceanic and Atmospheric Administration (NOAA)/ National Climatic Data Center (NCDC) Extended Reconstructed Sea Surface Temperatures (ERSST), version 3b (Smith et al. 2008), for SST and the Twentieth Century Reanalysis (20CR) project, version 2 (Compo et al. 2011), for specific humidity and winds, both with a $2° \times 2°$ spatial resolution.

b. CMIP5 model simulations

Model simulations in this study include a multimodel ensemble from the WCRP CMIP5 models (Taylor et al. 2012) data output. Based on monthly data availability, including precipitation, specific humidity, and wind fields, we used all realizations of 35 models for historical simulations and future projections under the high-end RCP8.5 emission scenario. Altogether, 109 realizations were analyzed for the historical period and 72 realizations were analyzed for RCP8.5. For single-forcing simulations, we used all realizations of a common set of nine models for aerosol-forcing (27 realizations) and GHG-forcing (29 realizations) experiments. To avoid model bias, the results were compared with historical all-forcing simulations using the same nine models (45 realizations). Details of CMIP5 model simulations are provided in Table 1. All model output were interpolated to a $1° \times 1°$ spatial resolution for precipitation and $2° \times 2°$ for SST, specific humidity, and winds.

3. Methods

a. S/N maximizing EOF analysis

We applied S/N maximizing EOF analysis (Allen and Smith 1997; Venzke et al. 1999; Chang et al. 2000) to JJA seasonal average rainfall of the CMIP5 ensemble to extract the externally forced signal, as in Ting et al. (2009). To focus on long-term low-frequency changes, an 11-yr running average was applied to the JJA seasonal mean data prior to the analysis. Given the multimodel, multirealization ensemble, the total covariance matrix of the ensemble mean can be assumed as a sum of two linearly independent matrices, one for forced signal and one for internal variability (climate noise). We first determined the spatial structure of the internal modes of variability through an EOF analysis on the noise matrix, formed using the second century of rainfall anomalies in the preindustrial control run for each of the corresponding CMIP5 model in the analysis. These noise EOFs (retaining 80% of the total variance) were used to form a spatial prewhitening transformation matrix to filter the internal variability that was not removed by multimodel ensemble averaging, so that the spatial

TABLE 1. List of CMIP5 models and the number of realizations used in the study. Asterisks denote the common set of nine models examined for single-forcing simulations. (Expansions for model name acronyms are available at http://www.ametsoc.org/PubsAcronymList.)

Model	Historical	RCP8.5	Aerosol	GHG
ACCESS1.0	1	1	—	—
ACCESS1.3	1	1	—	—
BCC_CSM1.1	3	1	—	—
BCC_CSM1.1(m)	3	1	—	—
BNU-ESM	1	1	—	—
CanESM2*	5	5	5	5
CCSM4	6	6	—	—
CESM1(BGC)	1	1	—	—
CESM1(CAM5)	3	3	—	—
CMCC-CESM	1	1	—	—
CMCC-CM	1	1	—	—
CMCC-CMS	1	1	—	—
CNRM-CM5	10	5	—	—
CSIRO Mk3.6.0*	10	10	5	5
FGOALS-g2*	4	1	1	1
FIO-ESM	3	3	—	—
GFDL CM3*	5	1	3	3
GFDL-ESM2G	1	1	—	—
GFDL-ESM2M*	1	1	1	1
GISS-E2-H*	5	1	5	5
GISS-E2-R*	6	2	5	5
HadGEM2-CC	1	1	—	—
HadGEM2-ES	4	4	—	—
INM-CM4	1	1	—	—
IPSL-CM5A-LR*	6	4	1	3
IPSL-CM5A-MR	2	1	—	—
IPSL-CM5B-LR	1	1	—	—
MIROC-ESM	3	1	—	—
MIROC-ESM-CHEM	1	1	—	—
MIROC5	5	3	—	—
MPI-ESM-LR	3	3	—	—
MPI-ESM-MR	3	1	—	—
MRI-CGCM3	3	1	—	—
NorESM1-M*	3	1	1	1
NorESM1-ME	1	1	—	—

covariance in the ensemble average is largely due to forced change. The leading EOF mode of the ensemble mean gives the dominant forced signal. Using the S/N leading principal component (PC1) as the forced index, we construct the forced patterns of rainfall, moisture, circulation, and moisture budget fields using regression analysis. In obtaining the multimodel mean (MMM) in this study, we first computed the ensemble mean for each model and then performed multimodel ensemble average using each model's ensemble mean. While this method may be affected by the models with fewer realizations—models with only single realization, in particular, thus contribute toward larger amplitudes of internal fluctuations—it has a certain advantage in terms of reducing the risk of greatly biasing toward models with more ensemble members. We used all available

realizations instead of using just one realization for each model because it provides a much larger ensemble set to eliminate internal variability.

b. Moisture budget analysis

The atmospheric moisture budget equation (Trenberth and Guillemot 1995; Seager and Henderson 2013; Seager et al. 2010, 2014) gives the balance between $P - E$ and the convergence of the vertically integrated atmospheric moisture flux for monthly or longer time averages (Trenberth and Guillemot 1995). In pressure coordinates, the balance can be expressed as follows:

$$\overline{P} - \overline{E} = -\frac{1}{g\rho_w} \nabla \cdot \overline{\int_0^{p_s} \mathbf{u}q\, dp}, \qquad (1)$$

where P is precipitation, E is evaporation, g is gravitational acceleration, ρ_w is the density of water, p is pressure, p_s is surface pressure, $\mathbf{u}$ is the horizontal wind vector ($\mathbf{u} = u\mathbf{i} + v\mathbf{j}$), and q is specific humidity. Overbars represent monthly mean values. The vertical integral in Eq. (1) is calculated as the sum over pressure levels, so we rewrite Eq. (1) as

$$\overline{P} - \overline{E} \approx -\frac{1}{g\rho_w} \nabla \cdot \sum_{k=1}^{K} \overline{\mathbf{u}_k q_k} \overline{\Delta p_k}, \qquad (2)$$

where k is the vertical level with a total of K levels and Δp is the pressure thickness. Here the calculation is performed on pressure levels from 1000 to 200 hPa. The total K is 10 levels in CMIP5 models. We neglected submonthly variations of surface pressure since this introduces no significant error (Seager and Henderson 2013).

We then denote departures from monthly means with primes; therefore,

$$\mathbf{u} = \overline{\mathbf{u}} + \mathbf{u}' \quad \text{and} \quad q = \overline{q} + q'. \qquad (3)$$

Thus, the monthly mean moisture flux can be expressed as

$$\overline{\mathbf{u}q} = \overline{\mathbf{u}}\,\overline{q} + \overline{\mathbf{u}'q'}. \qquad (4)$$

Separating the moisture divergence term into contributions of mean flow term and submonthly transient eddies, Eq. (2) can be written as

$$\overline{P} - \overline{E} \approx -\frac{1}{g\rho_w} \nabla \cdot \sum_{k=1}^{K} \overline{\mathbf{u}}_k \overline{q}_k \overline{\Delta p_k} - \frac{1}{g\rho_w} \nabla \cdot \sum_{k=1}^{K} \overline{\mathbf{u}'_k q'_k}\, \overline{\Delta p_k}. \qquad (5)$$

For the Asian monsoon region, the mean moisture convergence term $-(g\rho_w)^{-1} \nabla \cdot \sum_{k=1}^{K} \overline{\mathbf{u}}_k \overline{q}_k \overline{\Delta p_k}$ tends to balance well with $\overline{P} - \overline{E}$, in terms of both climatology

and changes. Therefore, we focus on this term for further analysis. To gain more understanding of the mechanisms governing the changes in the moisture budget, we further separate the total changes in mean moisture convergence into those resulting from changes in specific humidity (the thermodynamic component) and those resulting from changes in circulation (the dynamic component), as in Seager et al. (2010, 2014),

$$\overline{\mathbf{u}} = \overline{\mathbf{u}}_c + \overline{\mathbf{u}}_a, \quad \overline{q} = \overline{q}_c + \overline{q}_a, \tag{6}$$

here we denote monthly climatological values with subscript c, calculated using the time period 1900–49 given the weak anthropogenic forcing during this period, and anomalies with subscript a. Then the mean moisture convergence term can be derived as follows:

$$
\begin{aligned}
-\frac{1}{g\rho_w}\nabla \cdot \sum_{k=1}^{K} \overline{\mathbf{u}}_k \overline{q}_k \overline{\Delta p}_k &= -\frac{1}{g\rho_w}\nabla \cdot \sum_{k=1}^{K} (\overline{\mathbf{u}}_{k,c} + \overline{\mathbf{u}}_{k,a})(\overline{q}_{k,c} + \overline{q}_{k,a})\overline{\Delta p}_k \\
&= -\frac{1}{g\rho_w}\nabla \cdot \sum_{k=1}^{K} \overline{\mathbf{u}}_{k,c}\overline{q}_{k,c}\overline{\Delta p}_k - \frac{1}{g\rho_w}\nabla \cdot \sum_{k=1}^{K} \overline{\mathbf{u}}_{k,c}\overline{q}_{k,a}\overline{\Delta p}_k \\
&\quad - \frac{1}{g\rho_w}\nabla \cdot \sum_{k=1}^{K} \overline{\mathbf{u}}_{k,a}\overline{q}_{k,c}\overline{\Delta p}_k - \frac{1}{g\rho_w}\nabla \cdot \sum_{k=1}^{K} \overline{\mathbf{u}}_{k,a}\overline{q}_{k,a}\overline{\Delta p}_k.
\end{aligned}
\tag{7}
$$

Taking the difference on both sides of Eq. (7) and ignoring the quadratic term by assuming small amplitude in perturbation quantity, the total change of the mean moisture convergence (δMC) can be approximated as follows:

$$
\begin{aligned}
\delta\left(-\frac{1}{g\rho_w}\nabla \cdot \sum_{k=1}^{K} \overline{\mathbf{u}}_k \overline{q}_k \overline{\Delta p}_k\right) &\approx \delta\left(-\frac{1}{g\rho_w}\nabla \cdot \sum_{k=1}^{K} \overline{\mathbf{u}}_{k,c}\overline{q}_{k,a}\overline{\Delta p}_k\right) \\
&\quad + \delta\left(-\frac{1}{g\rho_w}\nabla \cdot \sum_{k=1}^{K} \overline{\mathbf{u}}_{k,a}\overline{q}_{k,c}\overline{\Delta p}_k\right),
\end{aligned}
\tag{8}
$$

where the first term on the right-hand side represents the thermodynamic contribution (δTH), involving only changes in specific humidity q, and the second term represents the dynamic contribution (δDY), involving only changes in circulation $\mathbf{u}$. In this study, the change δ was calculated as the regression coefficient of the quantity onto the forced index (standardized S/N PC1).

4. Forced changes of Asian summer monsoon rainfall in CMIP5 models and observations

a. S/N maximizing EOF1 and PC1

The S/N maximizing EOF analysis was performed on the 11-yr running mean JJA seasonal mean land precipitation for the Asian monsoon region (5°–55°N, 60°–150°E) in the CMIP5 model ensemble. We used the time period 1901–2000 for historical and 2011–94 for RCP8.5. The spatial structures and principal components of the leading S/N EOF modes are given in Fig. 2. For the

historical period, the dominant signal is a drying trend across South and East Asian monsoon domains (Fig. 2a), explaining 47% of the total variance. The S/N PC1 (Fig. 2c) shows there is a sharp increasing trend of the drying signal from 1940 to the late 1960s followed by a relatively flat period afterward. For RCP8.5, there is a clear wetting signal over the entire region (Fig. 2b) with an almost linear trend throughout the twenty-first century (Fig. 2d). This first mode explains a high percentage (83%) of the total variance, indicating that the externally forced variability of Asian summer monsoon rainfall in the future can be well represented by this uniformly wetting trend.

b. Forced twentieth- and twenty-first-century rainfall changes and associated SST patterns

Figure 3 shows the observed (Fig. 3a) and model simulated (Fig. 3b) Asian summer (JJA) monsoon rainfall regressed onto standardized S/N PC1 using CRU data and CMIP5 historical ensemble, respectively, and CMIP5 RCP8.5 simulations (Fig. 3c). We chose the CRU data because of its relatively high station coverage with continuous rain gauge observations, as shown in Fig. 1b. Note that the color scales are different in Fig. 3 for observations, CMIP5 MMM historical simulations, and RCP8.5 future simulations in order to bring out more detailed structures in each case. While the observed regression associated with S/N PC1 (Fig. 3a) shows some similarities to the linear trend in Fig. 1b, it does indicate more drying trend overall, particularly for the region between 20° and 35°N, than that shown in the linear trend. The CMIP5 historical MMM (Fig. 3c), on the other hand, indicates a predominantly drying trend expanding from eastern China to northern India. The discrepancy between model
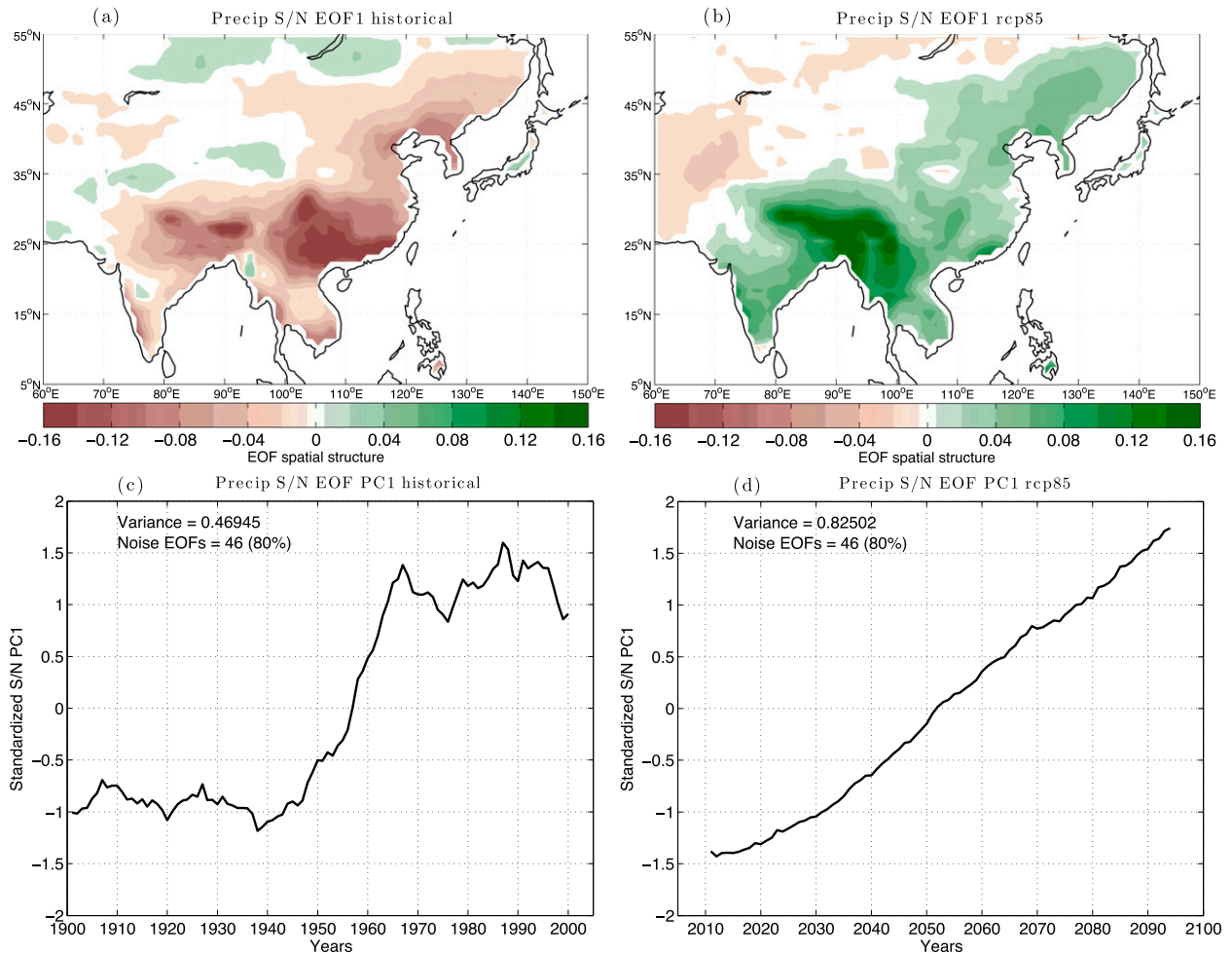
FIG. 2. First EOF mode of S/N maximizing EOF analysis of 11-yr running mean filtered JJA precipitation for CMIP5 (left) historical 1901–2000 and (right) RCP8.5 2011–94 simulations. (a),(b) Spatial structures and (c),(d) standardized leading principal components (S/N PC1).

simulations and observations lies in the regions south of 20°N and north of 35°N along the east coasts of Asia continent, where observations indicate a wetting trend and models showing mostly drying. It is not clear whether this discrepancy between model and observations is due to uncertainty in observations or model deficiencies. As for future model projected change under the RCP8.5 scenario (Fig. 3e), monsoon rainfall enhances across the entire Asian domain with relatively high model agreement.

The associated SST patterns (Figs. 3b,d,f), calculated as regressions of global SST onto the forced rainfall indices (standardized S/N PC1) display clear global warming trends in models and observations, aside from a strong cooling in northern North Atlantic in observations. There are, however, subtle differences in spatial patterns of SST in Fig. 3. As an example, the weak cooling off the east coast of China and Japan in Fig. 3d is not present in Figs. 3b,f. How much of the

regional SST features may have contributed to the differences in rainfall patterns in Fig. 3 will be explored in future studies. However, the overall agreement in SST patterns between models and observations in Fig. 3 suggests that the forced SST pattern may not be the dominant driver of the differences between modeled and observed historical precipitation trends or between modeled past and future precipitation trends.

5. Thermodynamic and dynamic mechanisms of twentieth- and twenty-first-century Asian summer monsoon changes

a. Changes in moisture content and monsoon circulation

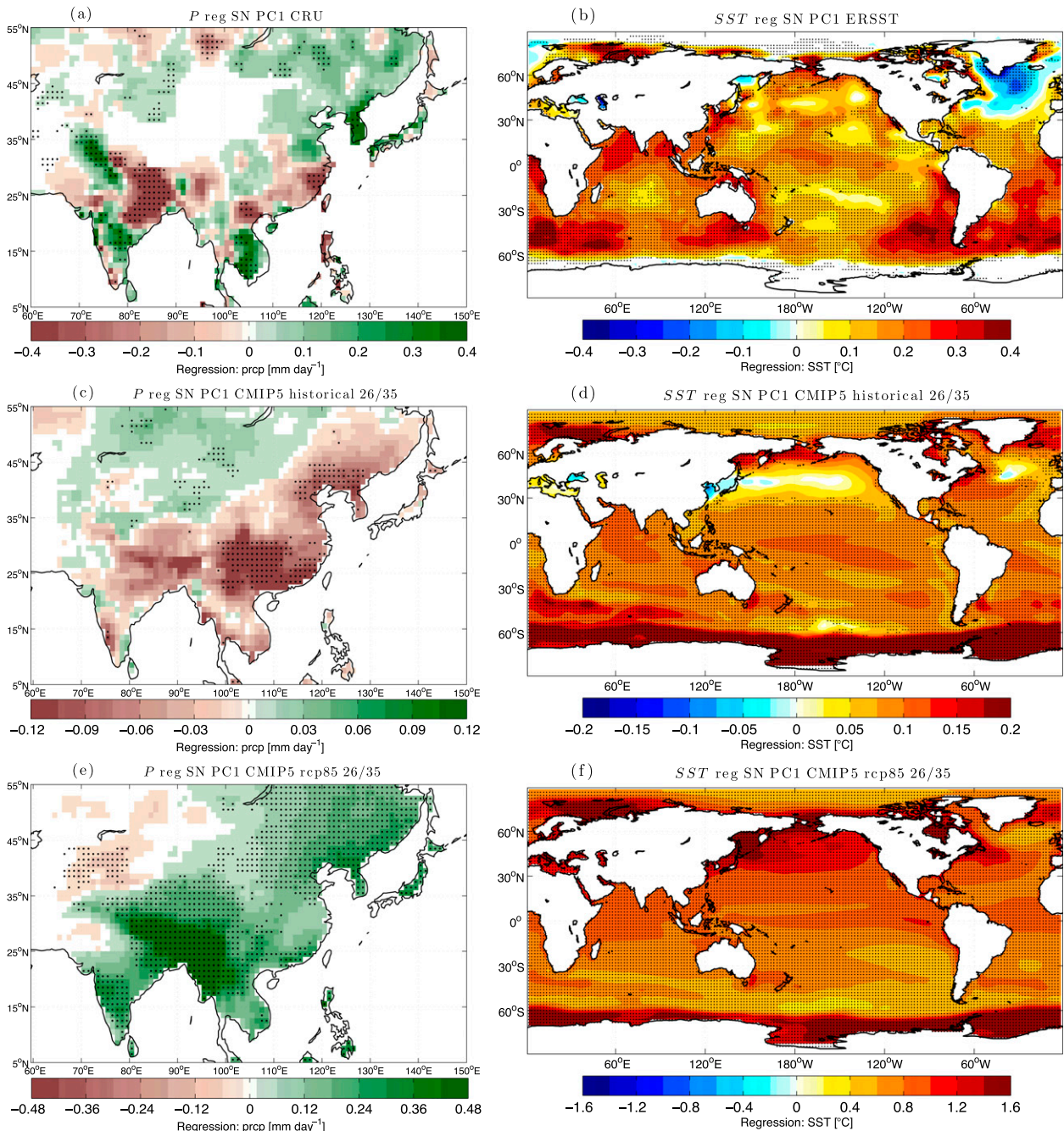To explore the physical processes leading to the monsoon rainfall change in CMIP5 models, we

FIG. 3. Regressions of JJA (a),(c),(e) precipitation (mm day^{-1}) and (b),(d),(f) global SST (°C) onto standardized S/N PC1 for (a),(b) observations 1901–2000 [CRU in (a) and ERSST in (b)], (c),(d) CMIP5 35-model MMM historical 1901–2000 simulations, and (e),(f) CMIP5 RCP8.5 2011–94 simulations. Stippling denotes 5% significance based on two-sided Student's t test in (a),(b) and 26 of 35 model agreement in (c)–(f).

examined moisture and circulation changes using 850-hPa specific humidity and horizontal wind fields, as shown in Fig. 4. In all cases, the lower troposphere moistens up as the temperature increases (Figs. 4a,c,e). The monsoon circulation intensifies in 20CR (Fig. 4b),

while CMIP5 models indicate reduced summer monsoon circulation for both Indian and East Asian monsoon in historical simulations (Fig. 4d). In the twenty-first-century RCP8.5 projections (Fig. 4f), the Indian monsoon circulation tends to be shifted northward
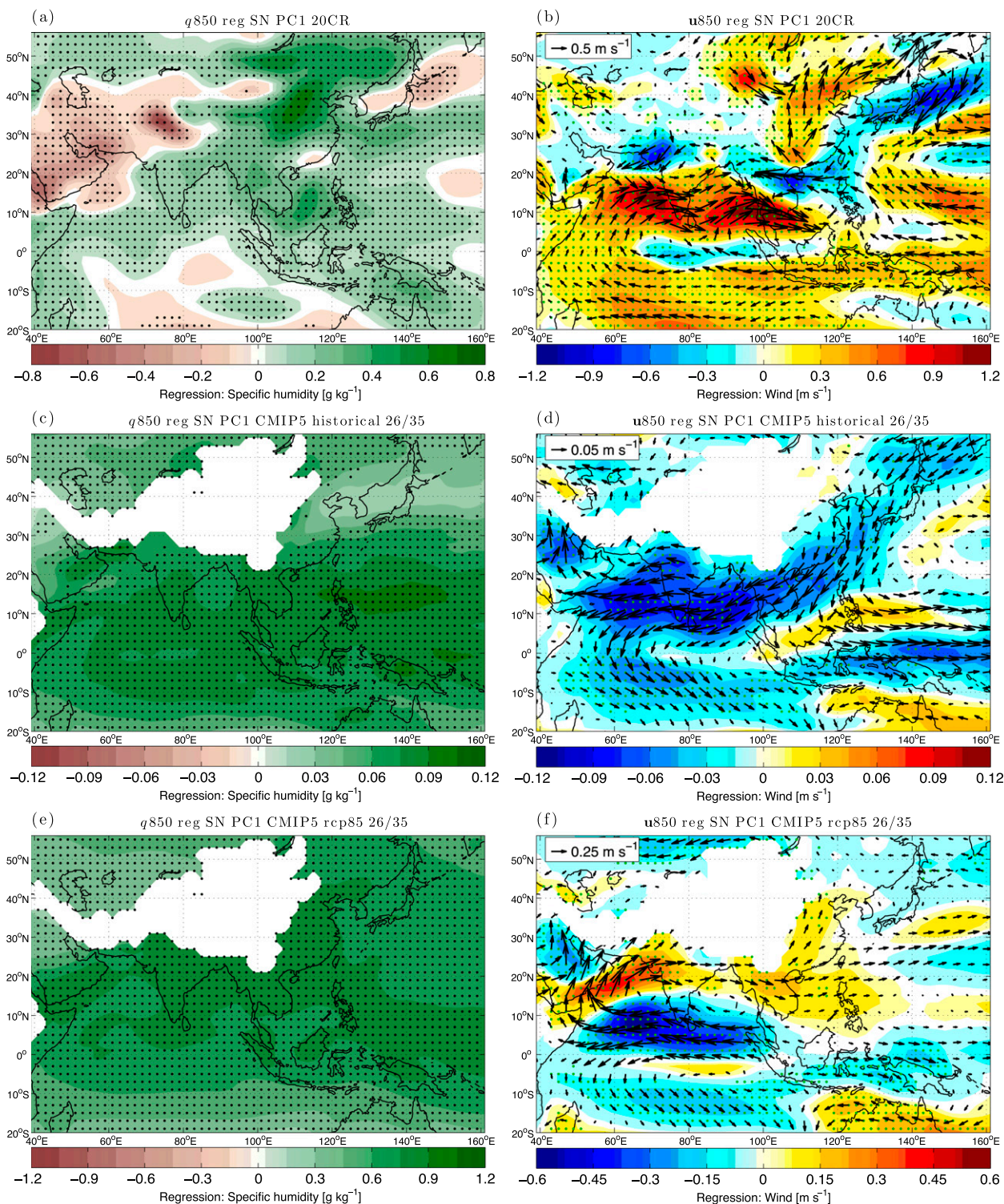
FIG. 4. Regressions of JJA (a),(c),(e) specific humidity (g kg^{-1}) and (b),(d),(f) wind (m s^{-1}) at 850 hPa onto standardized rainfall S/N PC1 for (a),(b) 20CR 1901–2000, (c),(d) CMIP5 35-model MMM historical 1901–2000, and (e),(f) CMIP5 RCP8.5 2011–94 simulations. In (b),(d),(f), arrows are vectors of regression coefficients of **u**; colors show the regression coefficients of wind velocity. Stippling denotes 5% significance based on two-sided Student's *t* test in (a),(b) and 26 of 35 model agreement in (c)–(f).

with a strong decrease in the south, while the East Asian monsoon circulation is enhanced.

The results in Fig. 4 indicate that the forced monsoon rainfall change is associated with a general increase in atmospheric moisture content for historical observations and model simulations, as well as for the future climate, whereas the monsoon circulation change differs in each of the three cases. This suggests that the differences in forced monsoon rainfall changes in Fig. 3 may have been caused by the discrepancies in the circulation responses. In observations, the increase of moisture and intensification of circulation both contribute toward the enhancement of monsoon rainfall. In historical model simulations, the weakened circulation may have dominated over the increased moisture content, resulting in an overall drying. However, in the twenty-first century, increasing water vapor as a result of greenhouse warming is much stronger than in the historical period (note that the color scale in Fig. 4e is an order of magnitude larger than in Fig. 4c), leading to greatly enhanced summer monsoon rainfall. These mechanisms will be further explored in the next subsection using moisture budget analysis within the CMIP5 modeling framework.

b. Changes in moisture budget

Figure 5 shows the regressions of $\overline{P} - \overline{E}$ (Figs. 5a,b), the mean moisture convergence (Figs. 5c,d), and the thermodynamic (Figs. 5e,f) and the dynamic (Figs. 5g,h) components of the mean moisture convergence, onto the standardized S/N PC1 for CMIP5 historical (left column) and RCP8.5 (right column) MMM. For both the historical and RCP8.5 model simulations, there is a good agreement between changes in $\overline{P} - \overline{E}$ and the mean moisture convergence (Figs. 5a,b), indicating a relatively minor contribution due to transient moisture convergence in the monsoon region. During the historical period in CMIP5, $\delta\overline{P} - \delta\overline{E}$ (Fig. 5a) and the total δMC (Fig. 5c) display a general drying pattern over the monsoon domain, consistent with the corresponding precipitation regression (Fig. 3c). There are general decreases in evaporation (not shown), resulting in a less negative and, in some areas, a slight positive $\overline{P} - \overline{E}$ change in Fig. 5a. The thermodynamic contribution to the mean moisture convergence change δTH (Fig. 5e) shows increasing moisture convergence while the dynamic contribution δDY (Fig. 5g) shows a strong decrease in moisture convergence. The overall decrease in mean moisture convergence in Fig. 5c indicates that the dynamic contribution (Fig. 5g) dominates over the thermodynamic contribution (Fig. 5e) during the historical period. Thus, the drying trend in the twentieth century is mainly due to the weakening monsoon circulation. For the future using the RCP8.5 scenario, on

the other hand, the increase in mean moisture convergence (Fig. 5d) is dominated by the increasing moisture convergence in the thermodynamic contribution (Fig. 5f), which shows a general increase in the Asian monsoon region, consistent with the rich-get-richer mechanism (Held and Soden 2006). The dynamic contribution (Fig. 5h) shows a weakened moisture convergence over the Asian monsoon region, indicating anomalous mass divergence in the region. The contributions of the dynamic component (Figs. 5g,h) are supported by the forced patterns of the 500-hPa vertical pressure velocity (ω) field (not shown), with anomalous descending motion in the monsoon region for both the historical period and RCP8.5. In summary, the discrepancies between the drying trend in the historical simulations and the wetting trend in the RCP8.5 future scenario can be explained by the relative importance of dynamic and thermodynamic contributions to the total mean moisture convergence. While the thermodynamic mechanism dominates in the future because of enhanced warming, the historical monsoon rainfall changes are dominated by the changes in monsoon circulation.

To further quantify the relative contributions of δTH and δDY, we examined the temporal evolution of the thermodynamic and dynamic terms in Eq. (7), averaged over land area of the major monsoon domain, 5°–35°N, 70°–122°E. The anomalies were calculated with respect to 1900–49 climatology. The MMM results for the 35 CMIP5 models are shown in Fig. 6 for historical 1900–2005 (Fig. 6a) and RCP8.5 2006–99 (Fig. 6b) simulations. An 11-yr running mean was applied to smooth the time series in order to emphasize the long-term trend. During the historical period, the dynamic component (blue line) exhibits a downward trend while the thermodynamic component (red line) trends upward. The evolution of the total mean moisture convergence anomaly (black line) is dominated by the dynamical weakening until the late 1960s, followed by a reversed trend due to the thermodynamic contribution from 1970 onward. For RCP8.5, the total mean moisture convergence follows the strong upward trend of the thermodynamic contribution with little change in the dynamic component of the moisture convergence. In both cases, the total mean moisture convergence (black line) balances well with the $\overline{P} - \overline{E}$ (green line), with minor departures resulting from the transient eddy contribution. It is clear that, in the future, the total mean moisture convergence, thus $\overline{P} - \overline{E}$, is predominantly controlled by the thermodynamic wet-get-wetter mechanism (Held and Soden 2006): the significant increase of water vapor content in the atmosphere associated with greenhouse warming leads to an enhanced hydrological cycle and the increase
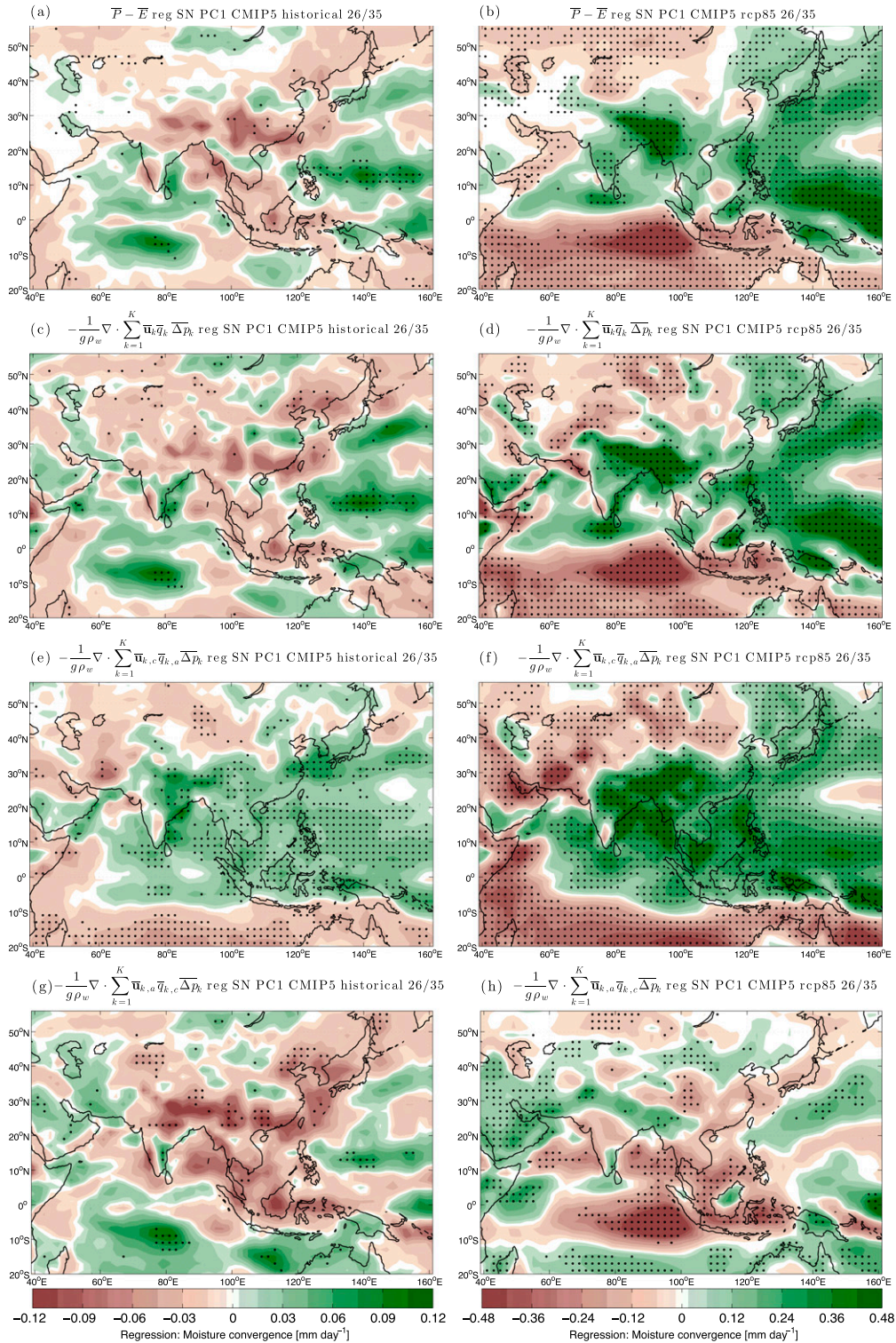
FIG. 5. Regressions of JJA (a),(b) $\overline{P} - \overline{E}$, (c),(d) the total mean moisture convergence, (e),(f) the thermo-dynamic component, and (g),(h) the dynamic component onto standardized rainfall S/N PC1 for CMIP5 35-model MMM (left) historical 1901–2000 and (right) RCP8.5 2011–94 simulations. Units for moisture convergence terms are millimeters per day. Stippling denotes 26 of 35 model agreement.
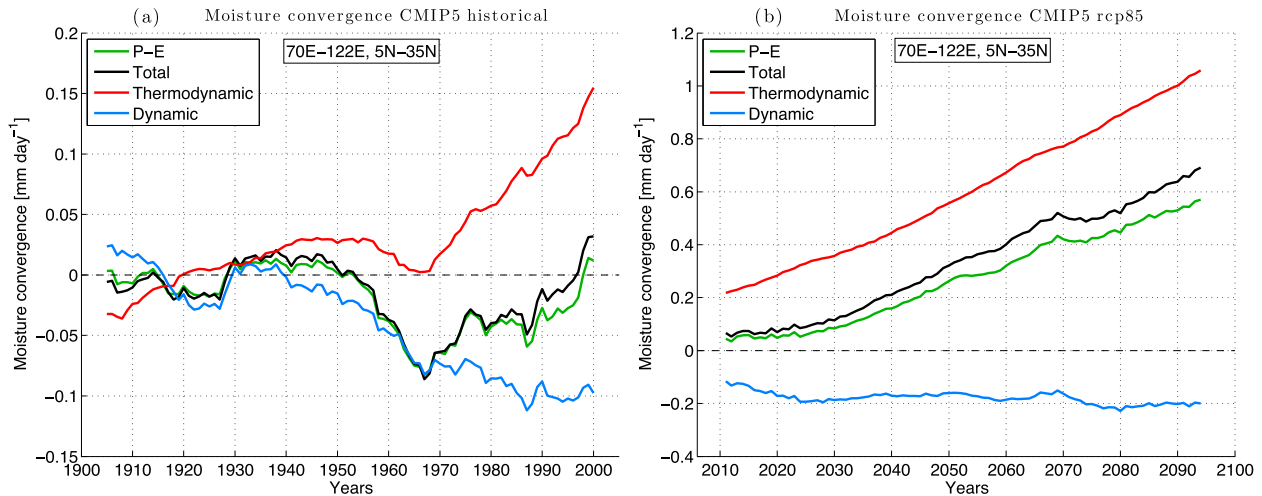
FIG. 6. Time series of area-averaged anomalies of JJA $\overline{P} - \overline{E}$ (green), the total mean moisture convergence (black), the thermodynamic component (red), and the dynamic component (blue) over land area within 5°–35°N, 70°–122°E for CMIP5 35-model MMM (a) historical 1900–2005 and (b) RCP8.5 2006–99. The anomalies are calculated with respect to 1900–49 climatology. The time series are smoothed with an 11-yr running average. Units are millimeters per day.

of monsoon rainfall. Previous studies have addressed the weakening tropical circulation as a robust response to a warmer climate (Vecchi and Soden 2007; Chadwick et al. 2013). Our results here indicate that the reduction of the dynamic component is small in the twenty-first century, which is consistent with the findings of Endo and Kitoh (2014), suggesting that the dynamical weakening of the Asian monsoon is less than that of other monsoons in future projections using both CMIP3 and CMIP5 models, possibly because of its distinctive geographical characteristics. It is interesting to note the reversal of the historical moisture convergence trend starting in the early 1970s in Fig. 6a, which coincides well with the flattening of the drying trend in the S/N PC1 in Fig. 2c. The strong drying trend between 1940 and 1970 in Fig. 2c can be largely attributed to the relatively weak increase in thermodynamic component but a large decrease in the dynamic component in Fig. 6a, which will be discussed in more detail in section 6.

6. Attributing historical changes to the relative roles of aerosols and GHGs

a. Twentieth-century rainfall changes forced by aerosols and GHGs

To examine the relative roles of aerosol and GHGs on monsoon change during the historical period, we further applied S/N maximizing EOF analysis to JJA rainfall on CMIP5 aerosol-only and GHG-only forcing runs using a common set of nine models (see Table 1). The dominant

mode in the all-forcing case using the nine models explains 49% of the total variance as compared to 47% in the case of using all 35 models (Fig. 2c). For the aerosol-only and GHG-only forcing cases, the first S/N EOF mode explains 54% and 34% of the total variance, respectively.

Regressions of rainfall onto the standardized S/N PC1 under all forcing (Fig. 7a), aerosol forcing (Fig. 7c), and GHG forcing (Fig. 7e) are shown in Fig. 7, as well as the standardized S/N PC1 indices (Figs. 7b,d,f). As illustrated by the regression plots, rainfall reduces under aerosol forcing (Fig. 7c) and increases under GHG forcing (Fig. 7e). The principal components display clear upward trends throughout the twentieth century. The total change (Fig. 7a) depends on the relative strengths of these two competing effects. Figure 7a suggests that aerosol forcing dominates over the greenhouse effect for the historical period and leads to the general drying trend in CMIP5's historical all-forcing simulations.

b. Changes in moisture content and monsoon circulation

We also examined 850-hPa specific humidity and wind fields to evaluate the thermodynamic and dynamic changes, as shown in Fig. 8. For moisture, lower-tropospheric water vapor reduces under aerosol effect (Fig. 8c) while enhancing greatly under greenhouse warming (Fig. 8e) as expected. The overall change in lower-tropospheric water vapor in the all-forcing scenario (Fig. 8a) is dominated by greenhouse warming. For the wind field, aerosols weaken the low-level monsoon circulation (Fig. 8d) while greenhouse effect shifts
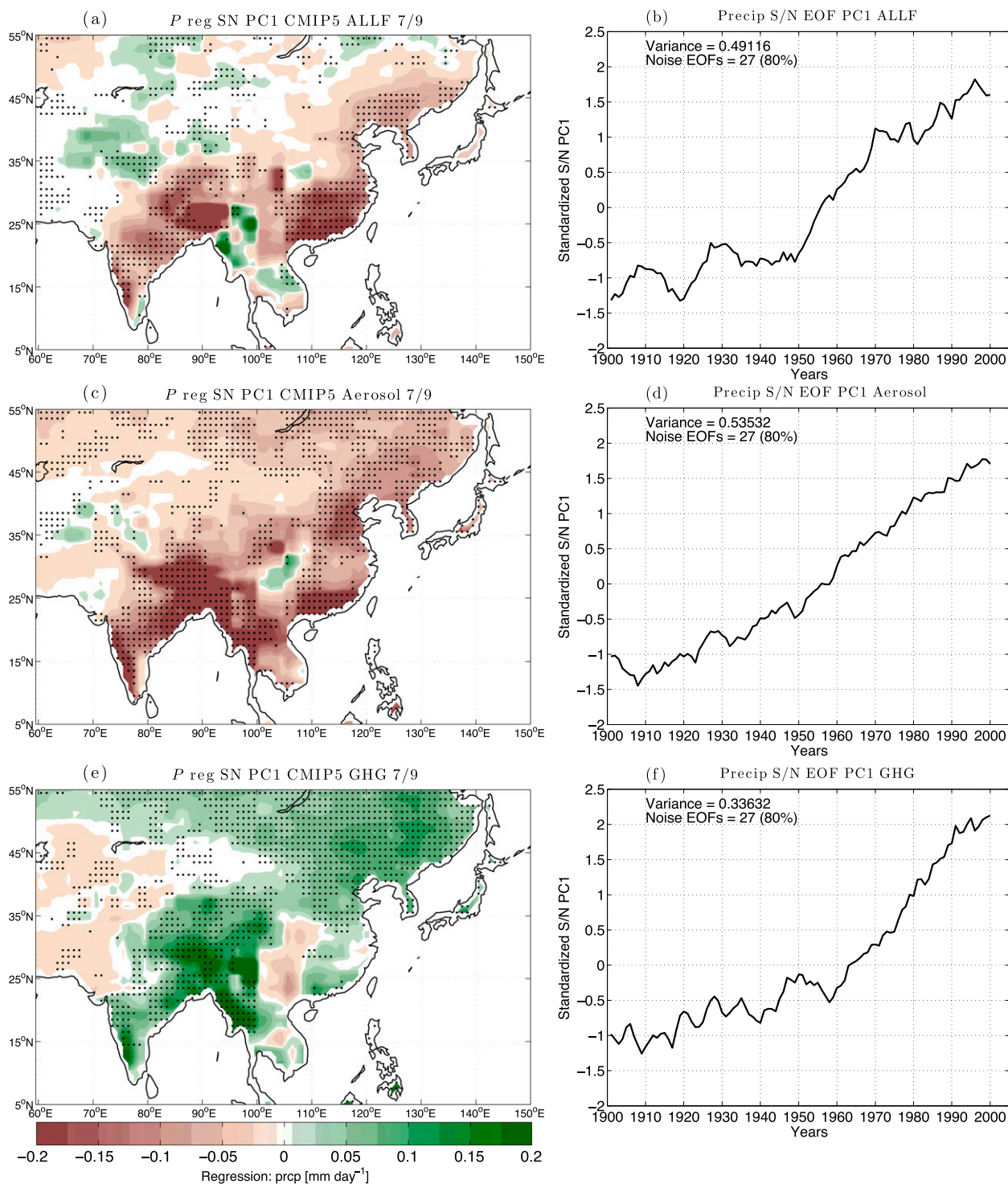
FIG. 7. (a),(c),(e) Regressions of JJA precipitation (mm day^{-1}) onto (b),(d),(f) standardized rainfall S/N PC1 from 1901 to 2000 for CMIP5 nine-model MMM historical (a),(b) all-forcing, (c),(d) aerosol-forcing, and (e),(f) GHG-forcing simulations. Stippling denotes 7 of 9 model agreement.
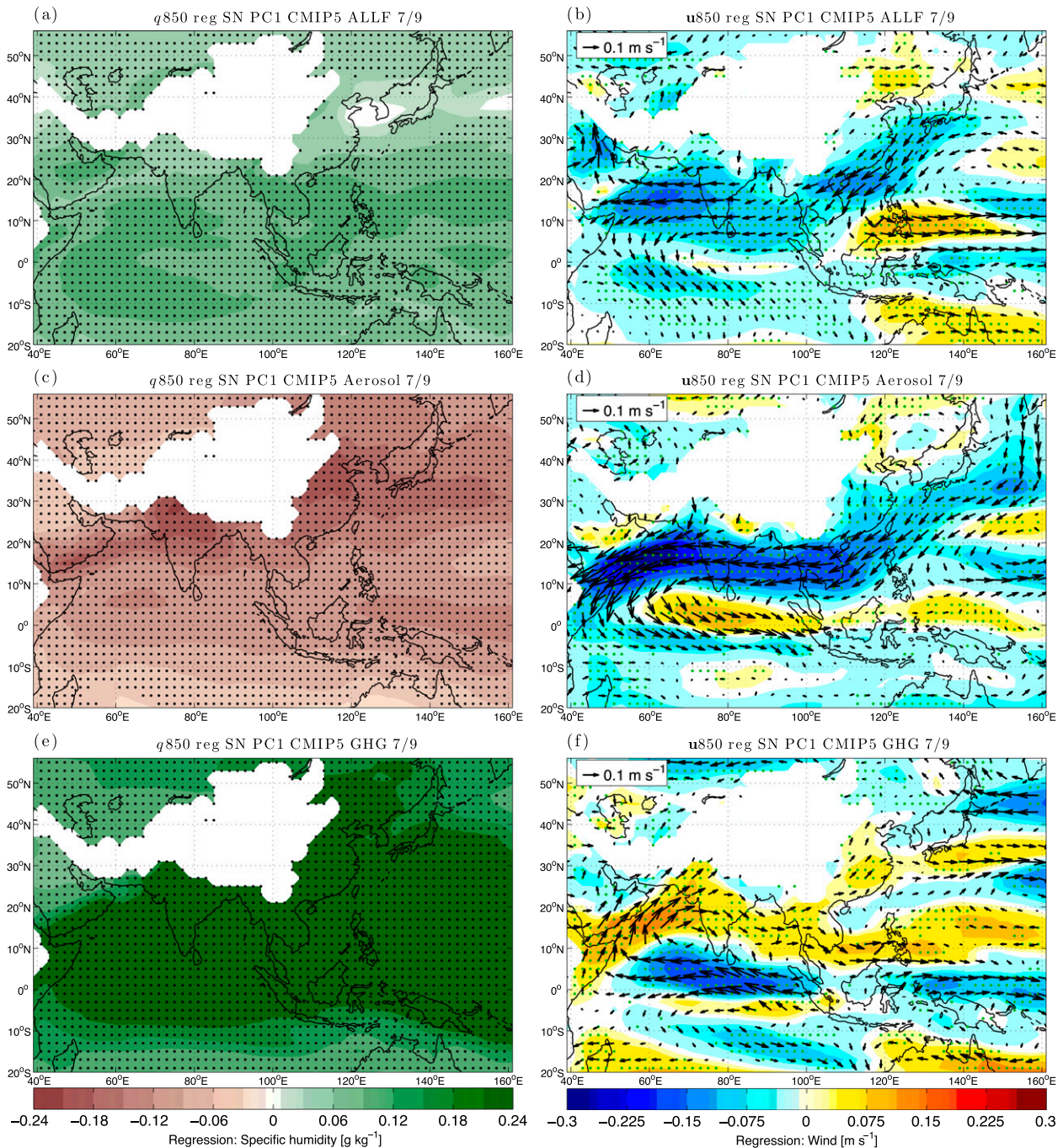
(a) q850 reg SN PC1 CMIP5 ALLF 7/9

(b) u850 reg SN PC1 CMIP5 ALLF 7/9

(c) q850 reg SN PC1 CMIP5 Aerosol 7/9

(d) u850 reg SN PC1 CMIP5 Aerosol 7/9

(e) q850 reg SN PC1 CMIP5 GHG 7/9

(f) u850 reg SN PC1 CMIP5 GHG 7/9

Regression: Specific humidity [g kg⁻¹]

Regression: Wind [m s⁻¹]

FIG. 8. As in Fig. 4, but for CMIP5 nine-model MMM historical (a),(b) all-forcing, (c),(d) aerosol-forcing, and (e),(f) GHG-forcing simulations from 1901 to 2000. Stippling denotes 7 of 9 model agreement.

Indian monsoon circulation northward and enhances East Asian monsoon circulation (Fig. 8f), similar to that for the RCP8.5 scenario in Fig. 4f. In this case, aerosol effect clearly dominates the monsoon wind change, resulting in weakened total monsoon circulation (Fig. 8b).

The roles of aerosol forcing and GHG forcing were further examined by taking the differences between all-forcing and GHG-forcing simulations and between all-forcing and aerosol-forcing simulations for the late twentieth century (1971–2005), respectively. The resulting monsoon rainfall and circulation differences (not
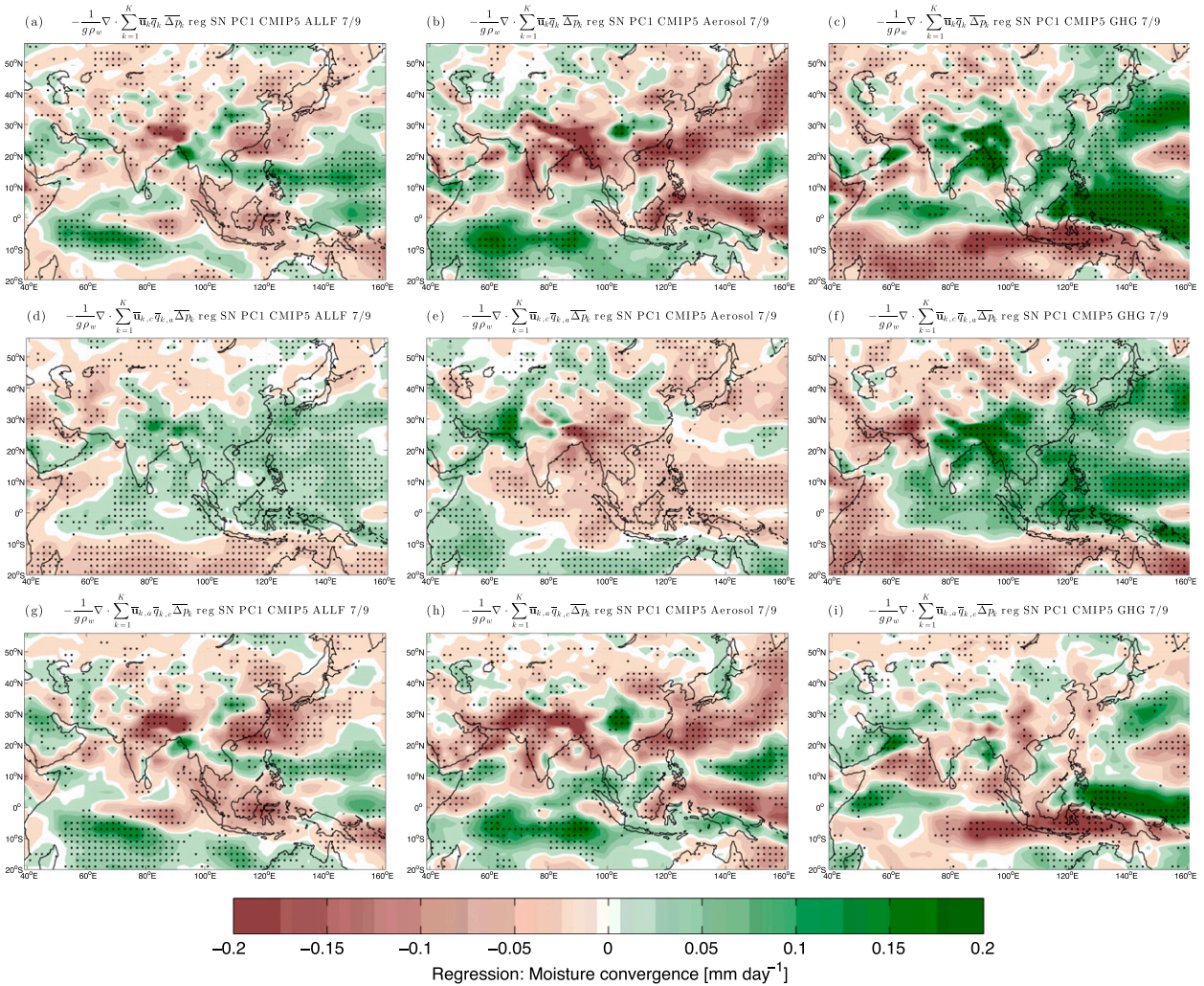
FIG. 9. Regressions of (a)–(c) JJA total mean moisture convergence, (d)–(f) the thermodynamic component, and (g)–(i) the dynamic component onto standardized rainfall S/N PC1 from 1901 to 2000 for CMIP5 nine-model MMM historical (left) all-forcing, (center) aerosol-forcing, and (right) GHG-forcing simulations. Units of the moisture convergence terms are millimeters per day. Stippling denotes 7 of 9 model agreement.

shown) are very similar to that in Figs. 7 and 8, confirming the robustness of the S/N EOF method for estimating the forced signals.

c. Changes in moisture budget

Figure 9 shows the spatial distribution of changes in moisture budget terms under all-forcing, aerosol-forcing, and GHG-forcing scenarios. The all-forcing (left column in Fig. 9) results are in gross agreement with those in Figs. 5c,e,g using a large set (35) of CMIP5 historical simulations, indicating that the results are relatively robust. Under aerosol forcing (center column in Fig. 9), δTH (Fig. 9e) and δDY (Fig. 9h) both show decreased moisture convergence over the monsoon domain, leading to the much reduced mean moisture

convergence (Fig. 9b). The dynamical weakening is particularly strong over India, Myanmar, as well as eastern China, while δTH is particularly strong over central China. Under GHG forcing (right column in Fig. 9), δTH (Fig. 9f) shows clearly enhanced moisture convergence across the monsoon domain, while δDY (Fig. 9i) indicates dynamical weakening over most parts of southern China, India, and Indo-China regions. The total δMC is predominantly driven by the thermodynamic enhancement, resulting in an overall strong convergence pattern (Fig. 9c). Consistent with Fig. 8, the thermodynamic change of mean moisture convergence in the all-forcing case (Fig. 9d) is dominated by the GHG forcing, while the dynamic change in mean moisture convergence in the all-forcing case (Fig. 9g) is

dominated by the aerosol forcing during the historical period.

One interesting feature in Fig. 9 is that the responses of the mean moisture convergence to aerosol forcing (Fig. 9b) and GHG forcing (Fig. 9c) over the western tropical Pacific and the Indian Ocean are very similar in spatial distribution but with opposite sign. Under aerosol (GHG) forcing, there is increased convergence (divergence) to the south of the equator over the Indian Ocean and increased divergence (convergence) at the Arabian Sea, Bay of Bengal, and most regions of the western Pacific. This is consistent with the findings of Xie et al. (2013), suggesting that the climate responses to aerosols and GHGs for both precipitation and SST are spatially similar and opposite in sign over the ocean, possibly because of the similar ocean–atmosphere feedbacks. However, our results indicate that the detailed mechanisms contributing to these opposite patterns in Figs. 9b,c may be quite different, with dynamic contribution dominating in the aerosol-forcing case and thermodynamic contribution dominating in the GHG-forcing case.

The relative importance of aerosols and GHGs was further examined by showing the temporal evolution of the area-averaged (land domain between 5° and 35°N and between 70° and 122°E) thermodynamic $[-(g\rho_w)^{-1}\mathbf{V}\cdot\sum_{k=1}^{K}\overline{\mathbf{u}}_{k,c}\overline{q}_{k,a}\overline{\Delta p_k}]$ and dynamic $[-(g\rho_w)^{-1}\mathbf{V}\cdot\sum_{k=1}^{K}\overline{\mathbf{u}}_{k,a}\overline{q}_{k,c}\overline{\Delta p_k}]$ terms under all-forcing, aerosol-forcing, and GHG-forcing scenarios. The all-forcing (Fig. 10a) temporal evolutions of the three moisture convergence terms are similar to that in Fig. 6a for 35 models but shown here for the nine models for direct comparison to the aerosol-only and GHG-only results. The aerosol-only case (Fig. 10b) shows a decreasing moisture convergence in both dynamic (blue) and thermodynamic (red) terms, resulting in a sharp decrease in the total mean moisture convergence (black). On the other hand, the thermodynamic component features a robust rising trend of moisture convergence under GHG forcing (red line in Fig. 10c), and a gradual decrease in the dynamic component (blue), resulting in a large increase in the total mean moisture convergence (black). It is suggested that the tropical meridional overturning circulation may slow down to compensate for the energy imbalance between the Northern and Southern Hemispheres induced by the hemispherically asymmetric anthropogenic aerosol emissions (Bollasina et al. 2011). The exact reason why there are large changes in atmospheric circulation (dynamic changes) because of anthropogenic aerosols as compared to the GHG forcing (Figs. 10b,c) will be explored in future studies using atmospheric general circulation model (AGCM) experiments.
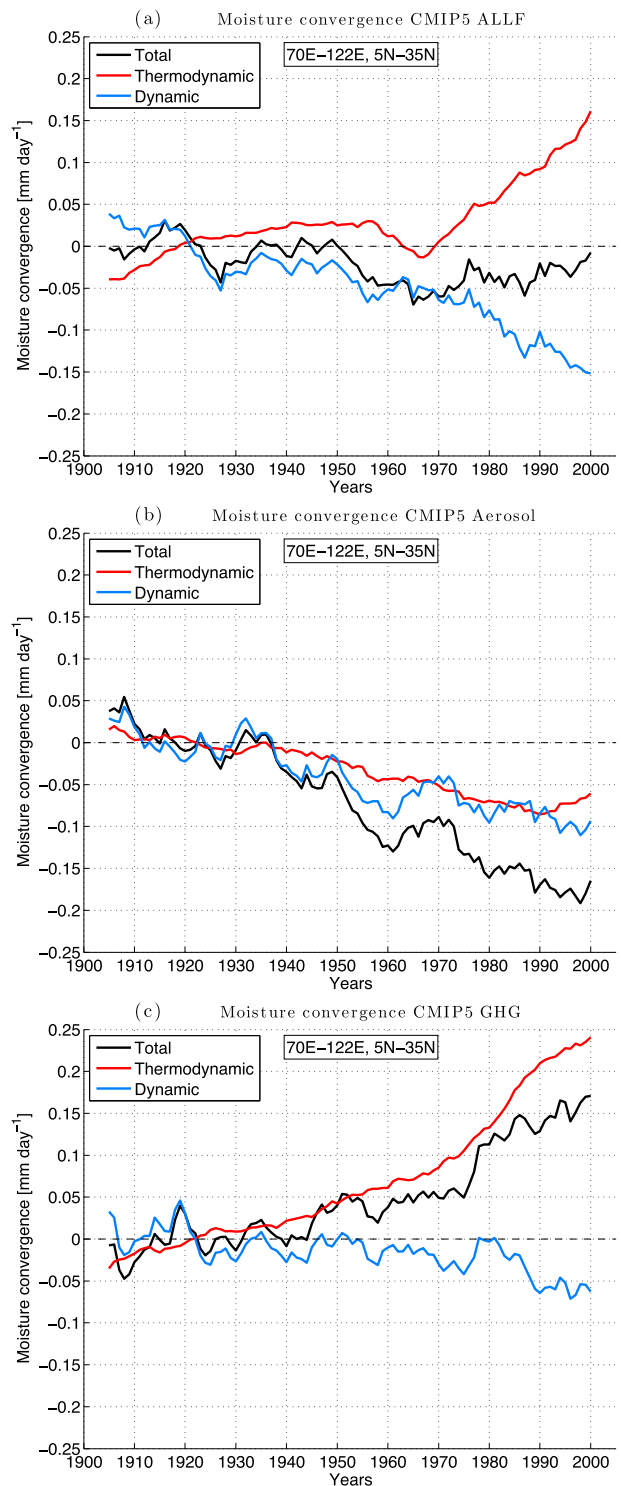

FIG. 10. Time series of area-averaged anomalies of JJA total mean moisture convergence (black), the thermodynamic component (red), and the dynamic component (blue) over land area within 5°–35°N, 70°–122°E for CMIP5 nine-model MMM historical (a) all-forcing, (b) aerosol-forcing, and (c) GHG-forcing simulations from 1900 to 2005. The anomalies are calculated with respect to the 1900–49 climatology. The time series are smoothed with an 11-yr running average. Units are millimeters per day.

The results in Figs. 9 and 10 confirm that aerosol forcing dominates the drying trend in the CMIP5 historical simulations through both dynamic and thermodynamic contributions. Given the discrepancies between observed and modeled historical monsoon rainfall trends, this raises the question of whether aerosol effect is appropriately represented in the CMIP5 models given the uncertainty in aerosol forcing as well as the aerosol indirect effect. It also questions whether the RCP8.5 scenario, which gradually phases out the aerosol forcing, is representative of the future aerosol emission in the Asian monsoon region and how this uncertainty may affect the monsoon rainfall future projections. Nevertheless, it is clear that reducing air pollution in the Asian monsoon region not only has the benefit of clean air but also can potentially levitate the drought threats over the monsoon region in the near future.

7. Summary

Using S/N maximizing EOF analysis on the CMIP5 multimodel, multirealization simulations, we extracted a model-based best estimate of the externally forced signal for Asian summer monsoon rainfall. The twentieth- and twenty-first-century changes of Asian summer monsoon in response to anthropogenic forcing were examined using both observational data and CMIP5 model simulations. Results show that in the twentieth century, CMIP5 models indicate a predominantly drying pattern expanding from eastern China to northern India. However, there are significant discrepancies when compared to the observed pattern. For the twenty-first century under the RCP8.5 scenario, monsoon rainfall enhances across the entire Asian domain.

We examined the thermodynamic and dynamic mechanisms causing these changes for both the historical and RCP8.5 scenarios using low-level specific humidity, wind, and the moisture budget analysis. Results reveal that the discrepancies between the drying trend in the CMIP5 historical simulations and the wetting trend in the RCP8.5 projections can be explained by the relative importance of dynamic and thermodynamic contributions to the total mean moisture convergence. While thermodynamic mechanism dominates in the future, the historical monsoon rainfall changes are dominated by the changes in monsoon circulation.

We further assessed the relative contributions of aerosols and GHGs on the twentieth-century monsoon change. Rainfall reduces under aerosol forcing and increases under GHG forcing; thus, the total change depends strongly on the relative strengths of these two competing effects. During the historical period, aerosol forcing dominates over the greenhouse effect, leading to

the general drying trend in CMIP5's historical all-forcing simulations. The thermodynamic change of mean moisture convergence in the all-forcing case is dominated by the GHG forcing, while the dynamic change in mean moisture convergence in the all-forcing case is dominated by the aerosol forcing during the historical period. Aerosol forcing dominates the drying trend in the CMIP5 historical simulations through both dynamic and thermodynamic contributions. It suggests that, in the near future, air pollution control policies will not only have the benefit of clean air but also potentially levitate the drought threats over the monsoon region.

Aerosol effect is one of the major uncertainties for climate models in simulating monsoon characteristics (Turner and Annamalai 2012). Our results here indicate that the modeled Asian monsoon change is largely dominated by the anthropogenic aerosols in the historical period. Thus, discrepancies in aerosol forcing between model and observations as well as among individual models may have contributed largely to differences in forced monsoon trends. In addition, the Asian monsoon region is poorly covered by station observations during the early part of the twentieth century, which leads to uncertainty in the observed pattern, especially over eastern China. Further modeling and understanding of the range of uncertainties associated with aerosol forcing and its impact on Asian monsoon changes is imperative for better hydroclimate projection in Asia.

REFERENCES

Allen, M. R., and L. A. Smith, 1997: Optimal filtering in singular spectrum analysis. *Phys. Lett.,* **234,** 419–428, doi:10.1016/S0375-9601(97)00559-8.

Annamalai, H., J. Hafner, K. P. Soorai, and P. Pillai, 2013: Global warming shifts the monsoon circulation, drying South Asia. *J. Climate,* **26,** 2701–2718, doi:10.1175/JCLI-D-12-00208.1.

Bollasina, M. A., Y. Ming, and V. Ramaswamy, 2011: Anthropogenic aerosols and the weakening of the South Asian summer monsoon. *Science,* **334,** 502–505, doi:10.1126/science.1204994.

Chadwick, R., I. Boutle, and G. Martin, 2013: Spatial patterns of precipitation change in CMIP5: Why the rich do not get richer in the tropics. *J. Climate,* **26,** 3803–3822, doi:10.1175/JCLI-D-12-00543.1.

Chang, P., R. Saravanan, L. Ji, and G. C. Hegerl, 2000: The effect of local sea surface temperatures on atmospheric circulation over the tropical Atlantic sector. *J. Climate,* **13,** 2195–2216, doi:10.1175/1520-0442(2000)013<2195:TEOLSS>2.0.CO;2.

Chou, C., J. D. Neelin, C.-A. Chen, and J.-Y. Tu, 2009: Evaluating the ''rich-get-richer'' mechanism in tropical precipitation change under global warming. *J. Climate,* **22,** 1982–2005, doi:10.1175/2008JCLI2471.1.

Christensen, J., and Coauthors, 2014: Climate phenomena and their relevance for future regional climate change. *Climate Change 2013: The Physical Science Basis,* T. F. Stocker et al., Eds., Cambridge University Press, 1217–1308.

Compo, G. P., and Coauthors, 2011: The Twentieth Century Reanalysis project. *Quart. J. Roy. Meteor. Soc.,* **137,** 1–28, doi:10.1002/qj.776.

Cook, E. R., K. J. Anchukaitis, B. M. Buckley, R. D. D' Arrigo, G. C. Jacoby, and W. E. Wright, 2010: Asian monsoon failure and megadrought during the last millennium. *Science,* **328,** 486–489, doi:10.1126/science.1185188.

Endo, H., and A. Kitoh, 2014: Thermodynamic and dynamic effects on regional monsoon rainfall changes in a warmer climate. *Geophys. Res. Lett.,* **41,** 1704–1711, doi:10.1002/2013GL059158.

Ganguly, D., P. J. Rasch, H. Wang, and J.-H. Yoon, 2012a: Climate response of the South Asian monsoon system to anthropogenic aerosols. *J. Geophys. Res.,* **117,** D13209, doi:10.1029/2012JD017508.

——, ——, ——, and ——, 2012b: Fast and slow responses of the South Asian monsoon system to anthropogenic aerosols. *Geophys. Res. Lett.,* **39,** L18804, doi:10.1029/2012GL053043.

Harris, I., P. Jones, T. Osborn, and D. Lister, 2014: Updated high-resolution grids of monthly climatic observations—The CRU TS3.10 dataset. *Int. J. Climatol.,* **34,** 623–642, doi:10.1002/joc.3711.

Held, I. M., and B. J. Soden, 2006: Robust responses of the hydrological cycle to global warming. *J. Climate,* **19,** 5686–5699, doi:10.1175/JCLI3990.1.

Hong, J., and J. Kim, 2011: Impact of the Asian monsoon climate on ecosystem carbon and water exchanges: A wavelet analysis and its ecosystem modeling implications. *Global Change Biol.,* **17,** 1900–1916, doi:10.1111/j.1365-2486.2010.02337.x.

Kitoh, A., H. Endo, K. Krishna Kumar, I. F. A. Cavalcanti, P. Goswami, and T. Zhou, 2013: Monsoons in a changing world: A regional perspective in a global context. *J. Geophys. Res.,* **118,** 3053–3065, doi:10.1002/jgrd.50258.

Krishna Kumar, K., K. Rupa Kumar, R. G. Ashrit, N. R. Deshpande, and J. W. Hansen, 2004: Climate impacts on Indian agriculture. *Int. J. Climatol.,* **24,** 1375–1393, doi:10.1002/joc.1081.

——, B. Rajagopalan, M. Hoerling, G. Bates, and M. Cane, 2006: Unraveling the mystery of Indian monsoon failure during El Niño. *Science,* **314,** 115–119, doi:10.1126/science.1131152.

Lau, K.-M., M.-K. Kim, and K.-M. Kim, 2006: Asian summer monsoon anomalies induced by aerosol direct forcing: The role of the Tibetan Plateau. *Climate Dyn.,* **26** (7–8), 855–864, doi:10.1007/s00382-006-0114-z.

Lau, N.-C., and M. J. Nath, 2006: ENSO modulation of the interannual and intraseasonal variability of the East Asian monsoon—A model study. *J. Climate,* **19,** 4508–4530, doi:10.1175/JCLI3878.1.

Lee, J.-Y., and B. Wang, 2014: Future change of global monsoon in the CMIP5. *Climate Dyn.,* **42** (1–2), 101–119, doi:10.1007/s00382-012-1564-0.

Lei, Y., B. Hoskins, and J. Slingo, 2011: Exploring the interplay between natural decadal variability and anthropogenic climate change in summer rainfall over China. Part I: Observational evidence. *J. Climate,* **24,** 4584–4599, doi:10.1175/2010JCLI3794.1.

Lin, H., and Z. Wu, 2012: Indian summer monsoon influence on the climate in the North Atlantic–European region. *Climate Dyn.,* **39** (1–2), 303–311, doi:10.1007/s00382-011-1286-8.

Liu, X., and M. Yanai, 2001: Relationship between the Indian monsoon rainfall and the tropospheric temperature over the Eurasian continent. *Quart. J. Roy. Meteor. Soc.,* **127,** 909–937, doi:10.1002/qj.49712757311.

Mirza, M. M. Q., 2011: Climate change, flooding in South Asia and implications. *Reg. Environ. Change,* **11,** 95–107, doi:10.1007/s10113-010-0184-7.

Mishra, V., B. V. Smoliak, D. P. Lettenmaier, and J. M. Wallace, 2012: A prominent pattern of year-to-year variability in Indian summer monsoon rainfall. *Proc. Natl. Acad. Sci. USA,* **109,** 7213–7217, doi:10.1073/pnas.1119150109.

O'Gorman, P. A., R. P. Allan, M. P. Byrne, and M. Previdi, 2012: Energetic constraints on precipitation under climate change. *Surv. Geophys.,* **33** (3–4), 585–608, doi:10.1007/s10712-011-9159-6.

Piao, S., and Coauthors, 2010: The impacts of climate change on water resources and agriculture in China. *Nature,* **467,** 43–51, doi:10.1038/nature09364.

Ramanathan, V., and Coauthors, 2005: Atmospheric brown clouds: Impacts on South Asian climate and hydrological cycle. *Proc. Natl. Acad. Sci. USA,* **102,** 5326–5333, doi:10.1073/pnas.0500656102.

Rodwell, M. J., and B. J. Hoskins, 1996: Monsoons and the dynamics of deserts. *Quart. J. Roy. Meteor. Soc.,* **122,** 1385–1404, doi:10.1002/qj.49712253408.

Schneider, U., A. Becker, P. Finger, A. Meyer-Christoffer, B. Rudolf, and M. Ziese, 2011: GPCC full data reanalysis version 6.0 at 0.5°: Monthly land-surface precipitation from rain-gauges built on GTS-based and historic data, doi:10.5676/DWD_GPCC/FD_M_V6_050.

Seager, R., and N. Henderson, 2013: Diagnostic computation of moisture budgets in the ERA-Interim reanalysis with reference to analysis of CMIP-archived atmospheric model data. *J. Climate,* **26,** 7876–7901, doi:10.1175/JCLI-D-13-00018.1.

——, N. Naik, and G. A. Vecchi, 2010: Thermodynamic and dynamic mechanisms for large-scale changes in the hydrological cycle in response to global warming. *J. Climate,* **23,** 4651–4668, doi:10.1175/2010JCLI3655.1.

——, H. Liu, N. Henderson, I. Simpson, C. Kelley, T. Shaw, Y. Kushnir, and M. Ting, 2014: Causes of increasing aridification of the Mediterranean region in response to rising greenhouse gases. *J. Climate,* **27,** 4655–4676, doi:10.1175/JCLI-D-13-00446.1.

Seo, K. H., J. Ok, J. H. Son, and D. H. Cha, 2013: Assessing future changes in the East Asian summer monsoon using CMIP5 coupled models. *J. Climate,* **26,** 7662–7675, doi:10.1175/JCLI-D-12-00694.1.

Smith, T. M., R. W. Reynolds, T. C. Peterson, and J. Lawrimore, 2008: Improvements to NOAA's historical merged land-ocean

surface temperature analysis (1880–2006). *J. Climate,* **21,** 2283–2296, doi:10.1175/2007JCLI2100.1.

Song, F., T. Zhou, and Y. Qian, 2014: Responses of East Asian summer monsoon to natural and anthropogenic forcings in the 17 latest CMIP5 models. *Geophys. Res. Lett.,* **41,** 596–603, doi:10.1002/2013GL058705.

Takahashi, K., 2009: Radiative constraints on the hydrological cycle in an idealized radiative–convective equilibrium model. *J. Atmos. Sci.,* **66,** 77–91, doi:10.1175/2008JAS2797.1.

Taylor, K. E., R. J. Stouffer, and G. A. Meehl, 2012: An overview of CMIP5 and the experiment design. *Bull. Amer. Meteor. Soc.,* **93,** 485–498, doi:10.1175/BAMS-D-11-00094.1.

Ting, M., Y. Kushnir, R. Seager, and C. Li, 2009: Forced and internal twentieth-century SST trends in the North Atlantic. *J. Climate,* **22,** 1469–1481, doi:10.1175/2008JCLI2561.1.

Trenberth, K. E., and C. J. Guillemot, 1995: Evaluation of the global atmospheric moisture budget as seen from analyses. *J. Climate,* **8,** 2255–2272, doi:10.1175/1520-0442(1995)008<2255: EOTGAM>2.0.CO;2.

Turner, A. G., and H. Annamalai, 2012: Climate change and the South Asian summer monsoon. *Nat. Climate Change,* **2,** 587–595, doi:10.1038/nclimate1495.

Ueda, H., A. Iwai, K. Kuwako, and M. E. Hori, 2006: Impact of anthropogenic forcing on the Asian summer monsoon as simulated by eight GCMs. *Geophys. Res. Lett.,* **33,** L06703, doi:10.1029/2005GL025336.

Vecchi, G. A., and B. J. Soden, 2007: Global warming and the weakening of the tropical circulation. *J. Climate,* **20,** 4316–4340, doi:10.1175/JCLI4258.1.

Venzke, S., M. R. Allen, R. T. Sutton, and D. P. Rowell, 1999: The atmospheric response over the North Atlantic to decadal changes in sea surface temperature. *J. Climate,* **12,** 2562–2584, doi:10.1175/1520-0442(1999)012<2562:TAROTN>2.0.CO;2.

Wang, B., R. Wu, and X. Fu, 2000: Pacific–East Asian teleconnection: How does ENSO affect East Asian climate? *J. Climate,* **13,** 1517–1536, doi:10.1175/1520-0442(2000)013<1517: PEATHD>2.0.CO;2.

——, S.-Y. Yim, J.-Y. Lee, J. Liu, and K.-J. Ha, 2014: Future change of Asian-Australian monsoon under RCP 4.5 anthropogenic warming scenario. *Climate Dyn.,* **42** (1–2), 83–100, doi:10.1007/s00382-013-1769-x.

Wu, L., H. Su, and J. H. Jiang, 2013: Regional simulation of aerosol impacts on precipitation during the East Asian summer monsoon. *J. Geophys. Res.,* **118,** 6454–6467, doi:10.1002/jgrd.50527.

Xie, S.-P., C. Deser, G. A. Vecchi, J. Ma, H. Teng, and A. T. Wittenberg, 2010: Global warming pattern formation: Sea surface temperature and rainfall. *J. Climate,* **23,** 966–986, doi:10.1175/2009JCLI3329.1.

——, B. Lu, and B. Xiang, 2013: Similar spatial patterns of climate responses to aerosol and greenhouse gas changes. *Nat. Geosci.,* **6,** 828–832, doi:10.1038/ngeo1931.